

## All-optical processing in coherent nonlinear spectroscopy

Dan Oron, Nirit Dudovich, and Yaron Silberberg

*Department of Physics of Complex Systems, Weizmann Institute of Science, Rehovot 76100, Israel*

(Received 1 December 2003; published 31 August 2004)

In spectroscopy, the fingerprint of a substance is usually comprised of a sequence of spectral lines with characteristic frequencies and strengths. Identification of substances often involves postprocessing, where the measured spectrum is compared with tabulated fingerprint spectra. Here we suggest a scheme for nonlinear spectroscopy, where, through coherent control of the nonlinear process, the information from the entire spectrum can be practically collected into a single coherent entity. We apply this for all-optical analysis of coherent Raman spectra and demonstrate enhanced detection and effective background suppression using coherent processing.

DOI: 10.1103/PhysRevA.70.023415

PACS number(s): 32.80.Qk, 42.65.Dr, 78.47.+p

Optical spectroscopy typically requires post-processing of the measured spectrum, where by correlation with known tabulated spectra the various measured lines are attributed to known substances. In incoherent spectroscopy, this is the only way to differentiate between contributions of various substances. This often requires detailed knowledge of line shapes and relative intensities and in many cases requires more experimental data. In contrast, coherent spectroscopy does not have to be limited to post-processing, due to the ability to induce interference between quantum paths involving several intermediate states. In the following we focus on application of this principle to coherent nonlinear Raman spectroscopy.

Coherent Raman processes have recently attracted considerable interest, in particular due to their potential for chemically sensitive microscopy of untreated biological specimen [1–3]. Still, despite the coherent nature of the process, the common wisdom of analysis of these spectra remained unchanged, practically neglecting the coherence properties of the signal. Here we exploit this coherence, taking advantage of the ability to induce interference between contributions from several vibrational levels. Rather than considering a single vibrational level at a time, we practically group a number of levels, which serve as a much better spectroscopic fingerprint, into a single entity. It should be noted that such grouping of lines has been applied to linear absorption spectroscopy using a tailored amplitude-modulated ultrashort pulse [4]. However, the ability to exploit interference in the case of a nonlinear process significantly increases the advantages of grouping. Groups of background lines can be practically eliminated from the Raman spectrum by destructive interference, while groups of signal lines are enhanced by constructive interference. This concept can be realized experimentally by phase-and-polarization coherent control, either in an open-loop or in an adaptive manner, of single-pulse coherent anti-Stokes Raman spectroscopy (CARS).

In CARS—the most commonly used scheme for coherent Raman spectroscopy—two photons with frequencies  $\omega_p$  (“pump”) and  $\omega_s$  (“Stokes”) excite a vibrational level at an energy  $\hbar(\omega_p - \omega_s)$ . A probe photon at  $\omega_{pr}$  interacts with the excited level to emit a signal photon at a frequency  $\omega_p - \omega_s + \omega_{pr}$ . Typically, two narrow-band beams (picosecond pulses,

matching the natural linewidth) are used, exciting only Raman levels in resonance with their energy difference [5]. When narrow-band pump and probe beams and a broadband Stokes beam are used, multiple Raman levels are excited, and the measured CARS spectrum resembles the spontaneous Raman spectrum, reflecting all transitions within the excitation bandwidth (“multiplex CARS”) [5].

Recently, we applied coherent control to perform single-pulse multiplex CARS [6], where all three photons driving the CARS process are provided by the same ultrashort pulse. In that work, all vibrational levels were excited impulsively by the main ultrashort pulse, while a single narrow spectral band around a frequency  $\omega_{pr}$  was split off the broadband excitation pulse for use as probe by shifting its polarization into the orthogonal axis. The resulting CARS signal induced by this probe is therefore composed of several spectral components, each associated with a particular vibrational frequency  $\Omega_R^n$  and centered at  $\omega_{pr} + \Omega_R^n$ , respectively. The instantaneous nonresonant background was eliminated by introducing a  $\pi$  phase shift at the center of the probe spectral band, eliminating the temporal overlap with the broadband pump.

In this work we show that a more complex and carefully designed probe pulse can facilitate all-optical processing of the entire vibrational spectrum. We construct a probe pulse containing contributions from several narrow spectral bands with controllable intensities and phases, as schematically illustrated in Fig. 1(a). The presence of several spectrally separated probe frequencies leads to strong interference effects in the CARS spectrum, as shown in Fig. 1(b). This interference pattern can be used in two ways to improve detectability in coherent Raman spectroscopy. When attempting to detect a given substance, coherent addition of the contributions from several vibrational levels can be performed, generating a total signal which is significantly larger than the linear sum of the separate contributions. When attempting to eliminate a resonant background it is possible to interfere destructively the contributions from several levels, resulting in a significant decrease of the background intensity.

We begin by characterizing the CARS signal driven by an electric field whose complex spectral amplitude is  $\epsilon(\omega)$ . For a singly resonant Raman transition through an intermediate

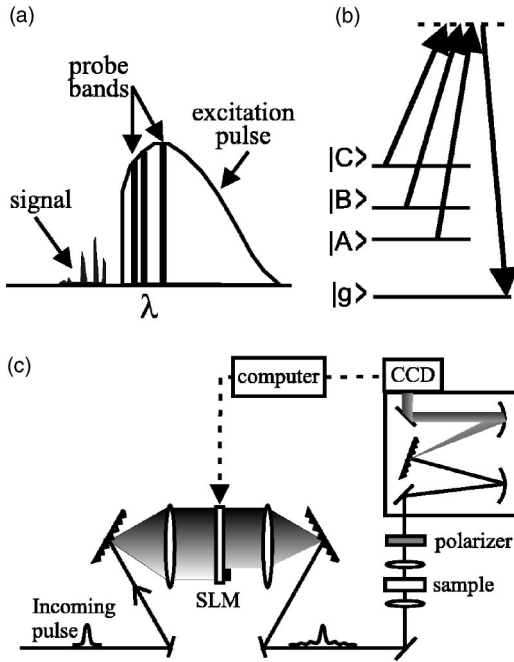


FIG. 1. Graphic description of the multiple-probe CARS process and the experimental setup. (a) Schematic description of the excitation pulse, blocked at its high-frequency (short-wavelength) end, the polarization-shifted spectral bands serving as probe in the CARS process, and the resulting signal. (b) Schematic description of the interference in the CARS spectrum when several Raman bands are excited and probed by correspondingly chosen narrow spectrum probe bands. (c) Schematic description of the experimental setup. The CARS signal at higher frequencies, blocked in the incoming pulse, is passed through a polarizer aligned along the probe pulse polarization and measured by a spectrograph and a cooled CCD.

level  $|i\rangle$  at an energy of  $\hbar\Omega_R$  and a bandwidth  $\Gamma$  we obtain [7]

$$P_j^{(3)}(\omega) \propto \chi_{jklm}^r \int_0^\infty d\Omega \frac{\epsilon_k(\omega - \Omega)}{(\Omega_R - \Omega) + i\Gamma} A_{lm}(\Omega), \quad (1)$$

where  $A_{lm}(\Omega) = \int_0^\infty d\omega \epsilon_j^*(\omega - \Omega) \epsilon_m(\omega)$  is the second-order polarization driving molecular vibrations and  $jklm$  denote the electric field polarizations.

Following Ref. [6] we consider the resonant CARS process where the molecular vibration is excited by a broadband pulse polarized along the  $x$  axis and probed by a pulse polarized along the  $y$  axis. We now derive an expression for the CARS signal under two conditions: the first is that there is no temporal overlap between the  $x$ -polarized pump and the  $y$ -polarized probe (i.e., the resonant  $\chi_{yxyx}$  term can be neglected and the nonresonant response vanishes), and the second is that  $A_{yy}$  is negligible. In practice, the conditions of the former can be achieved by phase control of the probe component [6] and the latter by shifting only a small portion of the pulse energy or a narrow spectral band to the probe polarization.

In this case the nonlinear polarization driving the  $y$ -polarized CARS signal can be approximated as

$$P_y^{(3)}(\omega) \propto \sum_n \chi_{yyxx}^n \int_0^\infty d\Omega \frac{\epsilon_y(\omega - \Omega)}{(\Omega_R^n - \Omega) + i\Gamma^n} A_{xx}(\Omega). \quad (2)$$

The summation goes over all resonant Raman transitions through intermediate levels at energies  $\hbar\Omega_R^n$  with bandwidths  $\Gamma^n$  and relative strengths  $\chi_{yyxx}^n$ .

If we now assume that the probe pulse is comprised of a number of narrow spectral bands of width  $\Delta$ , each centered at  $\omega_j$  and having an amplitude  $|C_j|$  and an overall phase  $\phi_j$ , as well as a phase flip at its center [6], we can write  $\epsilon(y)$  as

$$\epsilon_y(\omega) = \sum_j |C_j| e^{i\phi_j} \left[ \mathcal{R}\left(\frac{\omega - \omega_j - \Delta/4}{\Delta/2}\right) - \mathcal{R}\left(\frac{\omega - \omega_j + \Delta/4}{\Delta/2}\right) \right]. \quad (3)$$

where  $\mathcal{R}(x)$  denotes a rect function.

Assuming now that all linewidths  $\Gamma^n$  and the probe bandwidth  $\Delta$  are significantly smaller than the pulse bandwidth,  $A_{xx}(\Omega)$  can be taken out of the integral of Eq. (2), which can then be approximated as a double sum over all resonant Raman levels and probe bands:

$$P_y^{(3)}(\omega) \approx \sum_{j,n} \chi_{eff}^n |C_j| e^{i\phi_j} \delta(\omega_j + \Omega_R^n - \omega), \quad (4)$$

where  $\chi_{eff}^n = K_n \chi_{yyxx}^n A_{xx}(\Omega_R^n)$  and  $K_n$  is an order-unity coefficient evaluated from both the level linewidth and the probe bandwidth according to Eqs. (2) and (3) [8]. As can be seen in Eq. (4), there is symmetry between the vibrational levels and the narrow probe bands. Interference between contributions from several vibrational levels appears when the energy separation of the probe spectral bands equals the energy separation of the Raman levels, as shown schematically in Fig. 1(b).

We first demonstrate utilization of this interference pattern in CARS of several simple molecules in the liquid phase. Our experimental system consists of a mode-locked Ti:sapphire laser emitting 20-fs pulses at 80 MHz, a pulse shaper [9], and a spectrograph, as shown in Fig. 1(c). The pulse shaper is used both to apply the desired phase and polarization [10] to each frequency component of the pulse and to block the higher frequencies overlapping the CARS signal [6,11]. The sample is illuminated by pulses with a total bandwidth of 75 nm, equivalent to a span of about  $1100 \text{ cm}^{-1}$  and an energy of about 0.1 nJ. After passage through the sample, the excitation pulse is filtered out, and the CARS signal polarized parallel to the probe is measured. This system is suitable for CARS spectroscopy in the range of about  $300\text{--}900 \text{ cm}^{-1}$ , typical of carbon-halogen bond stretching. The lower limit stems from the technical requirement to filter out the excitation pulse, and the upper limit is due to the total bandwidth of the excitation pulse. The spectral resolution is about 0.5 nm, corresponding to about  $8 \text{ cm}^{-1}$ .

We first perform CARS of 1,2-dichloroethane, having three Raman levels in the measurable energy range. A CARS spectrum obtained using a single narrow-band probe at  $\omega_A$ , corresponding to  $\lambda = 782 \text{ nm}$ , is shown in Fig. 2(a) (following the method of Ref. [6]). The signals from the three Ra-

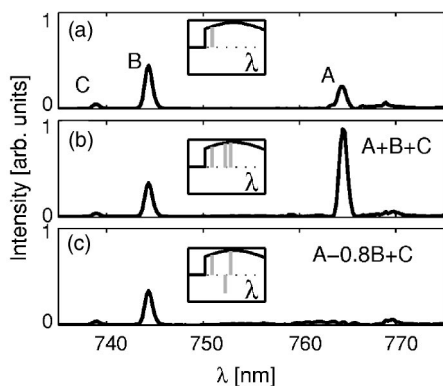


FIG. 2. CARS spectra from 1,2-dichloroethane. The insets denote the spectral masks used, where the excitation spectrum is shown in black and the polarization shifted probe bands are shown in gray. In practice, each of these probe bands has a width of 1.2 nm and a phase flip at its center, as defined in Eq. (3). The background due to birefringence of the objective lens has been subtracted from all the following spectra. (a) CARS spectrum using a single probe band (at 782 nm), showing three peaks corresponding to the Raman levels at  $298\text{ cm}^{-1}$  (A),  $652\text{ cm}^{-1}$  (B), and  $750\text{ cm}^{-1}$  (C). (b) CARS spectrum using a pulse with three probe bands (at 782, 804, and 811 nm, all in phase and fully  $y$  polarized) designed to induce constructive interference between the contributions of the three levels to the peak at 764 nm. Note that the peaks at 739 and 744 nm contain only a contribution from the probe band at 782 nm and are therefore almost unchanged relative to (a). (c) CARS spectrum using a pulse with three probe bands designed to induce destructive interference at 764 nm between the contributions of the three levels (in this case an additional  $\pi$  phase shift was applied to the probe band at 804 nm, inverting its overall phase, and the SLM was set to act as a  $0.35\lambda$  plate, so less energy is transferred to the  $y$  polarization).

man levels with energies of  $\Omega_A=298\text{ cm}^{-1}$ ,  $\Omega_B=652\text{ cm}^{-1}$ , and  $\Omega_C=750\text{ cm}^{-1}$  are marked as A, B, and C, respectively. The observed intensity ratios, reflecting  $\chi_{eff}$  for each level, are 4.5:9:1, respectively.

Consider first the case when we want to detect 1,2-dichloroethane more efficiently. To do so we shift two more spectral bands  $\omega_B$  and  $\omega_C$  to the probe polarization, so that  $\omega_A+\Omega_A=\omega_B+\Omega_B=\omega_C+\Omega_C$ . In this case the CARS signals from all three levels spectrally overlap at the spectral location of the A peak of Fig. 2(a). When all probe bands are in phase, constructive interference of all three contributions is achieved, as seen in Fig. 2(b). The observed ratio of the total A peak to the B peak is 2.6, significantly higher than the 1.6 ratio expected from an incoherent summation. It is still lower than the theoretical value for a coherent sum, 4.2, only due to the pixellization of the pulse shaper, which does not allow us to completely overlap the three contributions spectrally. The constructive interference significantly increases the detectability of weak Raman levels due to heterodyning with stronger ones. Moreover, the detection process does not require measurement of the entire CARS spectrum. Note that the two other peaks, B and C are nearly unchanged, since they are only due to the probe band at  $\omega_A$ . The slight decrease in their intensity is due to the somewhat smaller peak intensity of the pump pulse due to the additional probe bands.

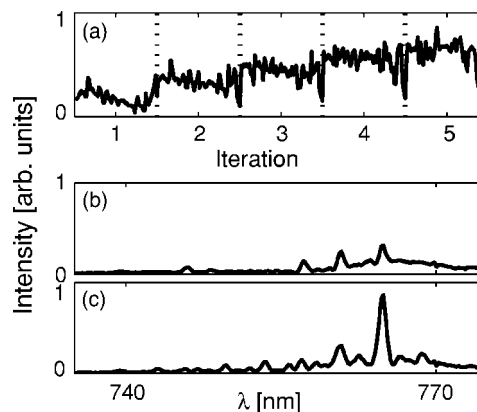


FIG. 3. An adaptive optimization of the signal at 765 nm from 1,2-dichloropropane. (a) The signal at 765 nm during the five iterations of the optimization procedure. The signal increases by about a factor of 3 from the peak of the first iteration (using a single probe band) to that of the fifth iteration (using five probe bands, all in phase with each other). (b) The measured CARS spectrum at the end of the first iteration. (c) The measured CARS spectrum at the end of the fifth iteration.

Consider now the case where 1,2-dichloroethane is a solvent in which we want to detect a low-concentration solute which has a Raman level overlapping one of the solvent levels. In this case we invert the phase of the probe band  $\omega_B$  and reduce its intensity by 20% by shifting less energy to the orthogonal polarization. The resulting CARS spectrum is shown in Fig. 2(c). The peak at 764 nm is completely eliminated due to destructive interference of the three levels. Note that other peaks in the CARS spectrum, where interference effects are not present, remain the same as in Fig. 2(b). This destructive interference is highly specific to the level structure of 1,2-dichloroethane. Any substance with a different line strength ratio of the three probed levels would thus generate a finite CARS signal at this spectral location.

Exact knowledge of the Raman level structure of the probed medium is often missing. This does not, however, limit the applicability of our method due to the availability of adaptive techniques [12]. In an adaptive search, we seek a pulse shape which maximizes some goal function. The measurement result is fed back into the computer which, using a search algorithm, decides on the next measurement. The goal function we choose is to maximize the total signal at 765 nm from a sample of 1,2-dichloropropane. Following the heuristics of a coherent addition of a number of separate bands, we choose a greedy optimization algorithm. In each iteration we add a single new probe band, keeping fixed all probe bands from previous iterations. The new spectral location is chosen to maximize the goal function, as long as it is spectrally separated from previous locations. The measured signal during five iterations is shown in Fig. 3(a). The measured CARS spectrum at the end of the first iteration (i.e., standard multiplex CARS) is given in Fig. 3(b). The measured CARS spectrum after five iterations is shown in Fig. 3(c). Here, the pulse contains five separate probe bands, corresponding to vibrational energies of 285, 352, 419, 623, and  $741\text{ cm}^{-1}$  (all  $\pm 8\text{ cm}^{-1}$ ), which indeed correspond to the five strongest Raman levels of 1,2-dichloropropane in the measured energy region.

Our experiment shows how coherent analysis of the Raman spectrum can be performed using shaped ultrashort pulses. The shaped pulse acts in an analogous manner to a matched filter in frequency domain, by use of which information on the correlation of the measured Raman spectrum with a given spectrum can be obtained. In particular, this method enables rejection not only of the nonresonant background, but also of the resonant background, due to an overlapping Raman level of the probed substance and the surrounding medium, a problem which has no solution to date. Using current-day laser systems this technique can be used to perform vibrational spectroscopy in the entire fingerprint spectral region [13] with a resolution of the order of typical Raman linewidths. The suggested method is particularly attractive for the detection of trace amounts of a substance in the presence of strong resonant Raman background. In fact,

the combination of adaptive pulse shaping with CARS has been recently suggested as a means to detect airborne contaminants such as bacterial spores [14]. It can also be applied to significantly improve the signal to background ratio in Raman optical biopsy, where small changes in ratios of chemical constituents within a cell are probed by changes in the relative strengths of Raman lines [15]. We believe this concept of utilizing the coherence properties of the Raman signal will have a significant impact on CARS microspectroscopy as well as on other coherent nonlinear spectroscopy applications.

The authors would like to thank Albert Stolow for stimulating discussions at the early stages of this work. Financial support of this research by the Israel Science Foundation is gratefully acknowledged.

- 
- [1] A. Zumbusch, G. R. Holtom, and X. S. Xie, *Phys. Rev. Lett.* **82**, 4142 (1999).
- [2] E. O. Potma, W. P. de Boeij, P. J. M. van Haastert, and D. A. Wiersma, *Proc. Natl. Acad. Sci. U.S.A.* **98**, 1577 (2001).
- [3] M. Muller, J. Squier, C. A. de Lange, and G. J. Brakenhoff, *J. Microsc.* **197**, 150 (2000).
- [4] W. S. Warren, *Proc. SPIE* **2124**, 78 (1994).
- [5] *Infrared and Raman Spectroscopy*, edited by B. Schrader (VCH, Weinheim, 1995).
- [6] D. Oron, N. Dudovich, and Y. Silberberg, *Phys. Rev. Lett.* **90**, 213902 (2003).
- [7] D. Oron, N. Dudovich, D. Yelin, and Y. Silberberg, *Phys. Rev. Lett.* **88**, 063004 (2002).
- [8] In practice, the  $\delta$  function of Eq. (4) has a width determined by the convolution of the Raman level linewidth and the bandwidth of each of the probe bands.
- [9] A. M. Weiner, *Rev. Sci. Instrum.* **71**, 1929 (2000).
- [10] T. Brixner and G. Gerber, *Opt. Lett.* **26**, 557 (2001); T. Brixner, G. Krampert, P. Niklaus, and G. Gerber, *Appl. Phys. B: Lasers Opt.* **74**, S133 (2002).
- [11] N. Dudovich, D. Oron, and Y. Silberberg, *Nature (London)* **418**, 512 (2002).
- [12] R. S. Judson and H. Rabitz, *Phys. Rev. Lett.* **68**, 1500 (1992).
- [13] N. Dudovich, D. Oron, and Y. Silberberg, *J. Chem. Phys.* **118**, 9208 (2003).
- [14] M. O. Scully *et al.*, *Proc. Natl. Acad. Sci. U.S.A.* **99**, 10994 (2002).
- [15] M. Gnaideka, H. C. Wulf, N. N. Mortensen, O. F. Nielsen, and D. H. Christensen, *J. Raman Spectrosc.* **28**, 125 (1997).